



HAL
open science

A rapid and simple protocol to prepare a living biocomposite that mimics electroactive biofilms

Stéphane Pinck, Mathieu Etienne, Manuel Dossot, Frédéric P.A. Jorand

► To cite this version:

Stéphane Pinck, Mathieu Etienne, Manuel Dossot, Frédéric P.A. Jorand. A rapid and simple protocol to prepare a living biocomposite that mimics electroactive biofilms. *Bioelectrochemistry*, 2017, 118, pp.131-138. 10.1016/j.bioelechem.2017.07.010 . hal-03561994

HAL Id: hal-03561994

<https://hal.science/hal-03561994>

Submitted on 8 Feb 2022

HAL is a multi-disciplinary open access archive for the deposit and dissemination of scientific research documents, whether they are published or not. The documents may come from teaching and research institutions in France or abroad, or from public or private research centers.

L'archive ouverte pluridisciplinaire **HAL**, est destinée au dépôt et à la diffusion de documents scientifiques de niveau recherche, publiés ou non, émanant des établissements d'enseignement et de recherche français ou étrangers, des laboratoires publics ou privés.



Distributed under a Creative Commons Attribution - NonCommercial - NoDerivatives 4.0 International License

A rapid and simple protocol to prepare a living biocomposite that mimics electroactive biofilms

Stéphane PINCK,^{1,2} Mathieu ETIENNE,^{1,2} Manuel DOSSOT,^{1,2} Frédéric JORAND^{1,2}*

¹CNRS, LCPME, UMR 7564, 405 rue de Vandoeuvre, F-54600 Villers-lès-Nancy, France.

²Université de Lorraine, LCPME, UMR 7564, 405 rue de Vandoeuvre, F-54600 Villers-lès-Nancy, France

*mathieu.etienne@univ-lorraine.fr

Abstract.

A living material was formed by self-assembly of bacterial cells (*Shewanella oneidensis* MR-1 or *Pseudomonas fluorescens*) with carbon nanotubes in the presence of cytochrome *c* from a bovine heart with the goal to mimic electroactive biofilms. The role of cytochrome *c* on self-assembly, cell viability and extracellular electron transfer was studied. Scanning electron microscopy and dynamic light scattering experiments highlighted its role on the self-assembly of bacteria-carbon nanotube aggregates within only 2 hours in solution. The deposition of these aggregates on glassy carbon surfaces led to a homogenous composite film in which the bacteria were embedded in a carbon nanotube network. A comparable cell density of 1 cell μm^{-2} was achieved in the presence or in the absence of cytochrome *c*, but this protein allowed maintaining a higher bacterial viability. Electrochemical characterization demonstrated the role of cytochrome *c* on electron transfer reactions, leading to a current density of up to 300 $\mu\text{A cm}^{-2}$ in the presence of 50 mM formate.

Keywords. Nanowire, artificial biofilm, *Shewanella oneidensis*, cytochrome *c*, carbon nanotube

1. Introduction

The ability of microorganisms to produce electricity by decomposing organic matter has been described for more than a century ago [1], however, without creating any significant interest for a long period of time [2,3]. The discovery of bacterial nanowires or conductive pili from *Shewanella oneidensis* MR-1 and [4] *Geobacter sulfurreducens* [5] has dramatically revived this topic and pushed forward the research on extracellular electron transfer (EET) in biofilms and their direct application in mediator-free microbial fuel cells [6]. Nowadays, many exciting research studies are striving to better characterize these nanowires [7–13] or propose new applications of bacterial biofilms for energy production [14], water treatment [15], commodity production [16] and biosensors [17].

Conductive pili from *S. oneidensis* MR-1 [8] and *G. sulfurreducens* [7] display different properties and involve different mechanisms for EET. Some recent results indicate that redox conductivity would be involved and not metallic-like conductivity [10]. A model is proposed in which the conductive pili operate coordinately with cytochromes [9]. With *S. oneidensis* MR-1, the conductive appendages are extensions of the outer membrane and periplasm that include the multiheme cytochromes involved in electron transfer reactions [8]. In addition to these systems, filamentous bacteria, acting as “living electrical cables”, were found responsible for electron conduction over cm in marine sediments [18]. To conduct electrons in some environments, nature has thus developed powerful strategies that we wish to control or mimic in some extent for biotechnological applications.

A major challenge is to facilitate electron transfer reactions between bacteria and electrodes. Malvankar and Lovley pointed out that increasing nanowire production in *G. sulfurreducens* biofilms led to improved current-producing capabilities in microbial fuel cells (MFC) [19]. So, bacterial strain selection or genetic manipulation are good strategies for improving EET [20]. Moreover, the power from MFC has been increased significantly over the past few years by gradually improving bioreactors [21], electrode materials [22], increasing the surface area, tuning the porosity [21] and modifying the surface with carbon nanomaterials [23] or selected chemical functions [24] and electron mediators [25].

Generally, biofilms from multi bacterial species are grown on the electrode surface for periods of time that can vary from days to weeks before reaching an optimal electrode response. Another approach involves the elaboration of a composite material made by mixing planktonic bacteria and exogenous materials that have not been self-produced by bacteria. A good example is the application of silica gel mimicking the extra-cellular polymeric substance (EPS) matrix to create standardized microbial fuel cell anodes [26]. An EET pathway between bacteria and electrode could even be improved in silica gel by using exogenous cytochrome *c*, in a system that can be considered as an artificial biofilm [27]. We define here an artificial biofilm as a man-made biocomposite, designed from the assembly of living bacterial cells with polymeric matrices, redox species (such as cytochromes) or conducting nanomaterials that mimic some functions of natural biofilms.

Electron transfer being one key issue, self-assembly of *S. oneidensis* MR-1 with graphene oxide has been proposed. The resulting macroporous biofilm had remarkable properties, delivering a 25-fold increase in the anodic current and a 74-fold increase in the cathodic one if compared to

the values for naturally occurring biofilms [28]. The EET can also be enhanced by biogenic nanoparticles [29].

Synthesis of bacterial composite materials is potentially a powerful approach for biotechnological applications such as synthetic biology [30], as it would allow rapid production of artificial biofilms [27], with engineered or selected strains [31]. The ideal route would be to directly involve planktonic bacteria cultivated in batch before immobilization under controlled and reproducible conditions. However, the factors inducing the synthesis by bacteria of conductive pili or other natural nanowires in biofilms are far from being understood. Therefore, controlling the nanowire production in bioelectrodes is not simple to realize. The introduction of artificial nanowires would be highly beneficial and would certainly furnish more opportunities for improving the EET with a variety of bacterial strains.

We report here a rapid method to produce a biocomposite film from planktonic bacteria and carbon nanotubes. The design of this bacterial composite was validated in this present study using planktonic *S. oneidensis* MR-1 and multi-walls carbon nanotubes (MWCNT) as a mimic of conductive pili. In addition, since electron conduction in biofilms naturally involves electron hopping between multiheme cytochromes [9,12,13] and considering the properties of cytochrome *c* (cyt *c*) which has been used as wiring agent in the field of bioelectrochemistry [32,33], we studied the role of cyt *c* from bovine heart as a model, in the EET effectiveness of the bacterial composite. We show that exogenous cytochrome molecules promote cell viability, organization of MWCNT with bacteria and EET. Self-assembly, cell viability and electron transfer reactions were evaluated by dynamic light scattering, scanning electron microscopy, confocal Raman spectroscopy, fluorescence imaging and electrochemistry.

2. Experimental

2.1. Reagents

Sodium formate (GC for analysis $\geq 99\%$; MERCK) and glucose (99 %, Acros) were used as electron donors for the bacterial cells. The multi-walled carbon nanotubes ($\geq 95\%$, MWCNT-COOH, outer diameter: 30 ± 10 nm, length: 1-5 μm) were purchased from Nanolab. Glassy carbon (SIGRADUR) was obtained from HTW Hochtemperatur-Werkstoffe GmbH (Germany) and graphite felt (GFD 4,6 E.A.) from SGL Group (Germany). The buffer and growth media were prepared from potassium chloride KCl solution ($\geq 99\%$, 1 mM, Sigma-Aldrich), trypticase soy broth (TSB-D, bioMérieux), trypticase soy agar (TSA-D, bioMérieux), lysogeny-broth (LB, Sigma-Aldrich) and phosphate buffer was prepared from 50 mM solutions of $\text{NaH}_2\text{PO}_4 \cdot 2\text{H}_2\text{O}$ ($\geq 99.6\%$; Prolabo) and $\text{Na}_2\text{HPO}_4 \cdot 2\text{H}_2\text{O}$ ($\geq 99\%$; Fluka). Cytochrome *c* bovine heart was purchased from Sigma-Aldrich ($\geq 95\%$). All solutions were prepared with high purity water (18 M Ω cm) from a Purelab Option water purification system (Elga LabWater, Veolia Water STI, Antony, France).

2.2. Bacterial strains and growth conditions

Escherichia coli CGE1 (environmental strain isolated from drinking water network) was from our laboratory collection, *Shewanella oneidensis* MR-1 (ATCC 700550) and *Pseudomonas fluorescens* (CIP 69.13) were from German or US collections, respectively. Each strain was streaked on plate culture medium from a glycerol stocks kept at $-80\text{ }^\circ\text{C}$. When needed, 0.1 mL of an overnight culture from a single colony on TSA-D was inoculated in 200 mL TSB-D and incubated at $30\text{ }^\circ\text{C}$ under stirring (160 rpm) for 48 h (*S. oneidensis* MR-1) and 24 h (*P. fluorescens*). Bacterial growth was measured by monitoring the optical density at 600 nm. *E. coli* was streaked on LB plates from stocks at $-80\text{ }^\circ\text{C}$. When needed, 0.1 mL of an overnight culture from a single colony was inoculated

in 200 mL LB and incubated at 37 °C under stirring (160 rpm) for 24 h. The culture was harvested by centrifugation at 5000 *g* for 10 min at room temperature. The pellet was washed twice with 1 mM KCl, and then suspended in 1 mM KCl in order to reach a cell density between 2×10^9 and 5×10^9 cell mL⁻¹ (determined by optical density measurement).

2.3. Electrode preparation and characterization

The bacterial cell suspension was mixed with the stock solution of cyt *c* (1 mM) and the stock suspension of MWCNT-COOH (5 mg mL⁻¹, dispersed in water by sonication for 30 min) in order to reach a final bacterial cell concentration of 1×10^9 cell mL⁻¹, a final cyt *c* concentration of 0.2 mM (or different if stated otherwise) and a final MWCNT-COOH concentration of 1 mg mL⁻¹. We did not observe an influence of the order of mixing on the experiments, however we always introduced MWCNT in the last step. The components of the suspension were allowed to self-assemble for 2 h. 10 μL of the final suspension was dropped on glassy carbon electrode (GCE) and allowed to dry at 4°C for 40 min. Another method of preparation was also used to reach a higher current density. In that case, 1.5 mL of the final suspension was deposited through a graphite felt (1.32 cm² geometric surface area). Measurements were done in an electrochemical cell containing 10 mL (CGE electrode) or 30 mL (graphite felt) of 50 mM PBS buffer (pH = 7) under stirring. In cyclic voltammetry experiments, the potential scan rate was 50 mV s⁻¹. In constant potential chronoamperometry, a potential of 0.35 V was applied to the biocomposite electrode. The counter electrode was a platinum wire and the reference electrode was Ag/AgCl 3M KCl.

2.4. Microscopy observation (SEM and epifluorescence)

To observe samples in epifluorescence microscopy, the LIVE/DEAD BacLight™ kit (Thermo Fischer Scientific) was used. Briefly, samples were mixed with DNA dyes SYTO 9 (1.67 μM) and

propidium iodide (1.67 μM) and incubated for 15 min before filtration (on 0.22 μm membrane filters). The filtrate was afterwards dropped on microscope glass slide and observed with an epifluorescence microscope (OLYMPUS BX51) with a magnification factor $\times 1000$. Samples analyzed by scanning electron microscopy (SEM) were prepared using two different methods. In the first one, the suspensions were filtered on 0.22 μm membrane filters and fixed afterward with glutaraldehyde 2.5% in sodium cacodylate buffer (pH 7.2). A washing step in sodium cacodylate buffer for 20 min was performed before a dehydrating step in an alcohol gradient for 70 min. After preparation, samples were dried and then metallized for the characterization with a Cambridge Stereoscan S240 SEM at an acceleration voltage of 1 kV. In the second one, the aggregates were dropped on a glassy carbon plate without any further preparation and observed with a Hitachi S-4800 SEM at an acceleration voltage of 1 kV.

4.5. Dynamic Light scattering

A Malvern Zetasizer 3000 HSA instrument was used to measure the size of particles in water by dynamic light scattering (DLS). Laser light was from a Helium-Neon laser with 5 mW of output power at 633 nm, and the scattered light was detected at 90° . The sample was introduced in a flow-through cell thermostated at 25°C . All the measurements were performed under suitable conditions by systematically diluting 50 times the samples with pure water in order not to saturate the detector, given the nature of aggregates. Water was first filtered with a mixed cellulose ester (surfactant-free) filter (0.45 μm of porosity). The attenuator (diaphragm) of the photomultiplier was automatically adapted for each sample in order to not saturate the detector. The data were analyzed by the CONTIN method [34]. Data are extracted from a global distribution in volume and the apparent diameter is the D50 value with its interquartile range (IQR) (see **Figure S1** for a visual representation of these data).

4.6. Raman Spectroscopy

In order to characterize interactions between the components, Raman spectroscopy analyses and Raman mapping experiments were performed. The spectra were obtained using a Jobin-Yvon T64000 triple-monochromator set-up equipped with a confocal microscope, a N₂-cooled CCD detector, a 1800 grooves mm⁻¹ grating, a frequency-doubled Nd: YAG laser with a wavelength of 530.53 nm. The spectral resolution was 1 cm⁻¹, the laser irradiance was kept below 5 kW cm⁻² to avoid heating of the sample. The back-scattered configuration was used with a X50 microscope objective (0.55 of numerical aperture). Raman mapping was realized on a Witec alpha 300 S set-up equipped with a cooled CCD detector, a frequency-doubled Nd: YAG laser with a wavelength of 532.26 nm and a 600 grooves mm⁻¹ grating. The spectral resolution was 4 cm⁻¹ and the reproducibility better than 0.5 cm⁻¹. The back-scattered configuration was used with a X100 long working distance microscope objective (0.90 of numerical aperture). The spatial resolution reached the diffraction limit and was estimated to be around 350 nm.

4.7. Cytochrome concentrations analysis

Cytochrome concentrations were determined by absorbance at 550 nm in a microplate reader (Infinite® 200, Tecan, Mannedorf, Switzerland). The amount of cytochrome in the biocomposite was deduced from cytochrome concentrations in supernatants after 2 h of self-assembly between *S. oneidensis* MR-1, MWCNT and cyt *c*. Sampling were performed in triplicate.

2. Results and discussion

The protocol to prepare the living biocomposite is summarized in **Scheme 1**. The individual elements of the biocomposite were mixed together in a solution and let to interact for two hours. Afterward, the suspension was deposited on an electrode surface, dried at 4 °C for 40 min and tested in solution as a functional material for electrocatalytic oxidation of formate.

S. oneidensis was cultivated and concentrated in order to achieve a cell density of 10^9 cells mL^{-1} . As such, the bacterial suspension was stable and no evidence of precipitation was observed during two hours in 1 mM KCl solution (**Figure 1A**, item a). The use of this medium prevented cell growth while protecting the bacteria from osmotic stress. Particle dimensions from the suspension could be estimated by dynamic light scattering (**Figure 1B**, a). The apparent diameter of bacteria was $1.6 \pm 0.4 \mu\text{m}$, which is consistent with the typical length of individual planktonic bacteria that have a rod-like shape, as confirmed by SEM showing cells displaying 1 to 3 μm length and 300 to 500 nm diameter (**Figure 2A**).

Multi-walled carbon nanotubes were chosen in this study as they are conductive and they display a length of 1-5 μm that is in the range reported for *S. oneidensis* nanowires [8]. However, the diameter of MWCNT used here (30 ± 10 nm) was bigger than that of nanowires from *Geobacter* (pili, ~ 3 nm) [7] and nanowires from *S. oneidensis* (membrane extensions, ~ 10 nm in dry conditions) [8]. An alternative would have been to use single-walled carbon nanotubes with a diameter of the order of 1 nm, but this material exhibit stronger cytotoxicity than multi-walled carbon nanotubes [35]. MWCNT-COOH were used in order to favor water dispersion and interactions with bacteria and proteins. A suspension of MWCNT at a concentration of 1 mg mL^{-1} in 1 mM KCl was stable and showed by DLS an apparent diameter of 300 ± 76 nm, *i.e.* much smaller than bacteria (**Figure 1**, item b). Note that this value does not correspond to either the diameter (30 nm) or the length of MWCNT (1-5 μm) because a DLS measurement simply provides

in that case an average size of the hydrodynamic beam of MWCNT and does not reflect their one-dimensional shape. An apparent diameter of $1.2 \pm 0.4 \mu\text{m}$ was found by mixing MWCNT with bacteria (**Figure 1**, item *c*), which was not significantly different from the average diameter of the bacteria alone. A careful analysis of the global distributions in **Figure S1** shows that this average diameter is not a simple combination of separated particles from a polydisperse suspension. The size distribution of bacteria is broader, resulting either from aggregation of MWCNT or from the interaction between bacteria and MWCNT that could possibly be deleterious, *e.g.* leading to cellular fragments or partially-lysed bacteria.

As cytochrome *c* can contribute to extracellular electron transfer reactions in biofilms produced from *S. oneidensis*, our first motivation was to incorporate exogenous cyt *c* (from bovine heart) in order to study its influence on the electrochemical response of artificial biocomposite films used as bioanode. This protein being positively charged at neutral pH (isoelectric point $\text{pI} = 10 - 10.5$), it could also promote electrostatic interactions between *S. oneidensis* and MWCNT, both being negatively charged on their outer surfaces in neutral conditions. However, the apparent diameter was only slightly increased by adding 0.2 mM cyt *c* to the bacterial suspension, reaching $2.0 \pm 0.3 \mu\text{m}$ after 2 h of interaction (**Figure 1**, item *d*). The influence of cyt *c* on the MWCNT suspension was more visible as the apparent average particle diameter increased up to $1.5 \pm 0.3 \mu\text{m}$ (**Figure 1**, item *e*), *i.e.* 5 times greater than the value for MWCNT alone (**Figure 1**, item *b*). The most dramatic effect was finally achieved after mixing together the three components, *i.e.* $10^9 \text{ cell mL}^{-1}$ bacteria, 1 mg mL^{-1} MWCNT and 0.2 mM cyt *c*. A precipitation was rapidly observed in the test tube resulting from an increase in the apparent diameter of the particles up to $6.0 \pm 2.5 \mu\text{m}$ after two hours (**Figure 1**, item *f*). Such a wide diameter range of particles could be explained by the method of preparation used to observe these samples in DLS that includes a dilution step. Cyt

c could thus act as a promoter of self-assembly between MWCNT and *S. oneidensis*. This putative mechanism could also involve MWCNT reorganization into bundles that is known to favor the adsorption of biological objects [36]. The kinetic of this phenomenon was monitored by following the increase in the apparent diameter of the assembly as a function of time, and it was found that large aggregates were produced after the first hour of reaction (**Figure S2**) and their size was not significantly changed during the second hour. Two hours of reaction time was later chosen for all the experiments reported in this work. The concentration of MWCNT was varied from 0.01 to 5 mg mL⁻¹ and the concentration of cyt *c* was changed from 0.01 to 1 mM and the optimal conditions determined on the base of this self-assembly process were the one analyzed here in details, i.e. 1 mg mL⁻¹ MWCNT, 0.2 mM cyt *c* and with 10⁹ cell mL⁻¹. For example, the optimal concentration of cyt *c* was determined by monitoring the remaining concentration of cyt *c* in the supernatant after 2 h interactions with 1 mg mL⁻¹ MWCNT and 1×10⁹ cell mL⁻¹. The experiment was performed with an initial concentration of cyt *c* ranging from 0.05 to 0.8 mM. Table 1 shows that no precipitation was observed in the presence of 0.05 or 0.1 mM cyt *c*, leading to high absorbance at 550 nm, due to the high optical density caused by the presence of bacteria and MWCNT. For higher concentrations of cyt *c*, an aggregation was observed, leading to the precipitation of the suspension (as illustrated in **Figure 1A**, item f). The quantity of cytochrome *c* adsorbed to bacteria and MWCNT was deduced from the concentration of cyt *c* remaining in the supernatant. The immobilized cyt *c* varies from 23×10⁻⁹ mole in the presence of 0.2 mM cyt *c* to 28×10⁻⁹ mole in the presence of 0.8 mM cyt *c*. Given the small differences in the cyt *c* adsorption with a concentration higher than 0.2 mM, this latter concentration was kept during all the studies.

The suspended particles were then analyzed by SEM after filtration on a nitrocellulose membrane with 0.2 μm porosity. The images obtained for *S. oneidensis* alone did not reveal any

particular connections between bacteria and no extra-cellular polymeric substance or fibrous structure were noted (**Figure 2A**). This would indicate that the bacteria did not produce bacterial nanowire in the culture conditions used in this study. On the contrary, the suspension containing both *S. oneidensis* and MWCNT clearly presented individual filaments connecting dispersed cells together (**Figure 2B**) and assumed to be MWCNT. Those connections could be the result of the drying step during SEM preparation as no significant aggregation was observed by DLS when MWCNT was mixed with *S. oneidensis* cells (**Figure 1** item c) The images of the suspension with the three components, *i.e.* *S. oneidensis* cells, MWCNT and cyt *c*, indicated the presence of a fibrous material surrounding the bacterial cells and connecting them together (**Figure 2C**). Considering the composition of the suspension this material must be composed of MWCNT, resulting from the self-assembly with bacterial cells in the presence of cyt *c*, which is consistent with the formation of aggregates observed by DLS in these conditions (**Figure 1** item f).

The self-assembly process was further analyzed by confocal Raman spectroscopy imaging (**Figure 3**). A five microliters drop of the suspension or solution was deposited on a microscope glass slide and left to dry. Raman spectra of cyt *c*, MWCNT and *S. oneidensis* were then collected individually (**Figure S3A-C**) aiming at identifying some characteristic bands of these individual components. In the spectral region 1000-1700 cm^{-1} , D and G band signals from MWCNT overlap with bands observed with cyt *c* and bacteria and cannot be used for their individual identification. Only the G' band at 2700 cm^{-1} could be used to unambiguously localize the MWCNT (**Figure S3C**). A small signal at 755 cm^{-1} was also found as a vibrational fingerprint of cytochromes, either bacterial (**Figure S3A**) or exogenous (**Figure S3B**). This signal has been ascribed in the literature to the pyrrole breathing mode ν_{15} [37]. Note that the intensity of the exogenous signal was about 10 times higher than that from bacteria, in these conditions.

The deposit obtained from the suspension with both MWCNT and cyt *c* from bovine heart (**Figure 3A-C**) was then studied. Heterogeneous and large patches were observed, larger than 10 μm in diameter, as shown in the center of the optical image (**Figure 3A**). The image at 2700 cm^{-1} shows that these large aggregates contain MWCNT. Carbon nanotubes were also found in a few other places at the surface, in the form of smaller aggregates (see area (b) in **Figure S4**). The imaging at 755 cm^{-1} permitted localizing cyt *c* and a similar image was found (**Figure 3B**). The good superposition of these two Raman images indicates that MWCNT and cyt *c* were co-localized in the sample within the aggregates (a spectrum collected in this area (a) is provided in **Figure S4**). We attribute the co-localization to the adsorption of positively-charged cytochrome molecules on the surface of negatively-charged MWCNT as has already been suggested in the literature [38].

In a second experiment, the suspension containing *S. oneidensis*, MWCNT and cyt *c* was dropped on the glass slide and dried. The optical image shows that this layer was homogeneous all over the surface (**Figure 3D**), as confirmed with a higher resolution SEM analysis (**Figure 4C**). Raman imaging at 2700 cm^{-1} indicates that MWCNT are better dispersed in the film with only a few brighter spots at some places (**Figure 3E**). Imaging at 755 cm^{-1} confirmed the homogeneity of the cytochrome distribution, also with visible bright spots (**Figure 3F**). A few areas were analyzed in more details. Circle areas (“c” on Fig 3D, E, F) show a large abundance of cytochrome while MWCNTs were not clearly visible (**Figure 3**, spectrum c). This result can be explained if we consider that cyt *c* in these areas was interacting with bacteria (more difficult to visualize) and not with MWCNT. In the same image, area (b) is characterized by the presence of both MWCNT and cyt *c* (spectrum b) and area (a) does not allow distinguishing signal peaks (spectrum a). It can be deduced that positively charged cyt *c* interacts with bacteria, notably through electrostatic interactions with the negatively charged outer membrane of the cells [39]. Self-assembly of

particles or biological elements are driven by nanoscale forces, including van der Waals, electrostatic and molecular surface forces, magnetic interactions and entropic effects [40]. We suppose that electrostatic forces would be here the driving force of the self-assembly observed between the negatively bacterial surface and the negatively charged MWCNT in the presence of exogenous *cyt c*.

To strengthen this hypothesis, two experiments were performed. Firstly, the ionic strength of the solution was increased by using 0.4 M phosphate buffer solution in place of 1 mM KCl. Whereas a precipitation was rapidly observed when the experiment was performed in 1 mM KCl (**Figure 1**, item f), it was not observed after 2 h in 0.4 M phosphate buffer, leading to a high absorbance at 550 nm due to interference caused by MWCNT and bacteria cells (**Table 1**). Indeed, if electrostatic forces are the driving forces of self-assembly, as we suppose, it must be hindered when ionic strength is increased. In the second test, the positively charged exogenous *cyt c* was replaced by bovine serum albumin (BSA) that is negatively charged in our experimental conditions (isoelectric point of BSA is 4.7 at 25 °C in water). While a precipitation was rapidly observed in the test tube containing positively charged *cyt c* with MWCNT and bacteria in 1 mM KCl (**Figure 1A**, item f), it was not observed in the presence of BSA (**Figure 1A**, item g). The suspension issued from bacteria mixed with MWCNT and BSA show an apparent diameter of $1.7 \mu\text{m} \pm 0.5 \mu\text{m}$ (**Figure 1B**, item g), not significantly different from the diameter measured with bacteria alone or mixed with MWCNT but clearly smaller than the diameter observed with the positively charged *cyt c*. To conclude, electrostatic forces could play a crucial role in the self-assembly process that we report here.

The produced aggregates could be thus considered as bricks to produce the artificial biofilm on electrodes. Scanning electron microscopy (SEM) was performed on the biocomposite deposited

on a glassy carbon surface resulting from the mixing of *S. oneidensis* with MWCNT (Figure 4A&B) and from the mixing of *S. oneidensis* with MWCNT and cyt *c* (Figure 4C&D). Rod-shaped bacteria are clearly visible in both samples and the large-scale imaging (Figure 4 B&D), which indicates that the surface densities are comparable, around 1.1 ± 0.2 cells cm^{-2} . Interestingly, when imaging these samples at higher magnification, a different apparent surface texture was observed: the bacterial shape on the biocomposite prepared in the absence of cyt *c* appears flat (Figure 4B) while in the presence of cyt *c* their shape was curved (Figure 4D). These different images suggest that positively-charged cyt *c* molecules influence the interaction between bacterial cells and MWCNT in a biocomposite layer deposited on a solid surface. Additional SEM images are provided in Supplementary Material that confirm the presence of carbon nanotubes and bacteria in the layer (Figure S5).

To assess the health of bacterial cells before their incorporation into the biocomposite, the live/dead® BacLight™ viability test was applied to the suspended bacteria after two hours of interaction with MWCNT. With this test, bacteria with a permeable membrane to the propidium iodide, are assumed to be dead or strongly altered, and conversely, they are considered to be alive when their cytoplasmic membrane is not permeable to the dye. As a control, a fresh bacterial suspension incubated by itself, resulted in 92 ± 4 % of intact cells (Table S1). In the presence of MWCNT, only 8 ± 4 % of the cells remained stable (Table S2). MWCNT cytotoxicity can be described by 3 mechanisms: a physical interaction between the cells and MWCNT resulting in the release of the intracellular content [41], an oxidative stress with reactive oxygenated species produced while the cells are in contact with MWCNT [42] and a toxicity provided by MWCNT impurities [43]. The addition of cyt *c* with MWCNT and bacteria in the suspension resulted in a net decrease of MWCNT toxicity upon bacteria, with 50 ± 4 % of intact cells (Table S3). The

physical interaction between cells and MWCNT is thus considered here as the most critical source of cytotoxicity; we suspect the self-assembly of MWCNT around bacteria in the presence of cyt *c* to promote cell viability by limiting membrane deterioration. And whatever the exact mechanism, these different results indicate that positively-charged cyt *c* molecules allow a protective interaction between bacterial cells and MWCNT in the biocomposite. This phenomenon was also favorable to extracellular electron transfer (EET) reactions that can be evaluated through electrochemical measurements.

A first insight into the electrochemical properties of the biocomposite deposited on glassy carbon electrodes was provided by cyclic voltammetry (CV). CV experiments with the biocomposite made of *S. oneidensis* and MWCNT showed only a poor electrochemical response with no clearly-defined current peaks (**Figure 5A**, curve a) that would have been related to outer-membrane cytochrome, free flavin or flavin bound to cytochrome [44]. In the presence of the exogenous cyt *c*, the cyclic voltammogram was dramatically changed with the appearance of a pair of redox peaks at 0.030 V (cathodic) and 0.125 V (anodic) versus Ag/AgCl (**Figure 5A**, curve b).

The existence of EET was observed in the presence of formate, an usual electron donor for the *Shewanella* strain. Electrons from formate oxidation are transferred to the outer membrane by the respiratory chain of the bacteria and flow out to the external acceptor, here the biocomposite electrode. A catalytic signal located at the potential of cyt *c* oxidation was clearly observed after addition of 0.3 mM formate in the solution (**Figure 5A**, curve c). We also observe a variation of the capacitive current measured with this electrode, possibly linked to changes in the living material during the measurement (curve c was measured approximately 20 min later than curve a). In a combined series of chronoamperometric experiments, a potential of 0.35 V versus Ag/AgCl was applied to the different electrodes, *i.e.* about 200 mV more positive than the peak potential of cyt

c oxidation so as not to be limited by electron transfer kinetics between cyt *c* and electrode materials (MWCNT and glassy carbon), and aliquots of 0.1 mM formate were spiked at three different times (**Figure 5B**). With the biocomposite prepared with bacteria and MWCNT, in the absence of exogenous cyt *c*, EET was observed but the maximum current was limited to 0.15 $\mu\text{A cm}^{-2}$ (**Figure 5B**, curve a). The introduction of cyt *c* into the biocomposite then allowed increasing EET as characterized by the rapid increase of current when formate was delivered to the bacteria up to a current density of 2.7 $\mu\text{A cm}^{-2}$ (**Figure 5B**, curve b). As expected, the current intensity was of the same order of magnitude and slightly lower than the Faradaic current measured by cyclic voltammetry using 50 mV s^{-1} scan rate (5.1 μA , curve c of Figure 5A). The experiment is well reproducible with a mean current density of $2.5 \pm 0.3 \mu\text{A cm}^{-2}$ calculated from four independent biocomposite electrode prepared from four independent batch of *Shewanella oneidensis*. The protein thus provided a protection to the bacteria that allowed maintaining a sufficient fraction of living cells which could then transfer electrons to the neighboring MWCNT network. This currents were more than 10 and 4 times higher than those measured with electrodes prepared with suspensions containing only bacteria (**Figure S6A**) or bacteria and cyt *c* (**Figure S6B**), respectively. Thus, cyt *c*, in combination with MWCNT, could increase EET both through structural organization of the components in the biocomposite and by electron shuttling.

Similar biocomposites were then prepared with *Escherichia coli* and *Pseudomonas fluorescens* (**Figure S7**). *E. coli* cannot allow extracellular electron transfer as it does not possess any outer-membrane cytochrome. This is indeed confirmed electrochemically as no current increase was observed upon successive additions of 5 mM glucose in the solution (Figure S7A). On the contrary, an increase in current was observed upon successive additions of 0.5 mM glucose with the biocomposite film prepared with *P. fluorescens* (Figure S7B). This bacterial species

possesses an outer membrane cytochrome but, contrary to *S. oneidensis*, to our knowledge it has not been reported to produce conductive nanowires. This experiment illustrates the great potential of bacterial biocomposite materials as it provides a rapid and effective way to efficiently connect electroactive bacteria, even those that would not be as efficient as *S. oneidensis* or *G. sulfurreducens* to transfer electrons over long distances in naturally grown biofilms.

The current density generated by the artificial biofilm could be further improved by depositing the biocomposite on a porous graphite felt electrode: up to $300 \mu\text{A cm}^{-2}$ in the presence of 50 mM formate (Figure 5C, curve a), thus approaching the current that can be encountered with biofilms naturally produced on electrodes over long periods of time [14]. A control experiment observed with applying the same protocol to *Shewanella oneidensis* show only a negligible current response (Figure 5C, curve b). One advantage of the method proposed in this report is that the biofilm was produced in about two hours, a short time on the scale of biofilm formation. This is the main interest of artificial biofilms made from a biocomposite material, the achievement in a short time and under controlled conditions of what nature needs to do slowly or cannot do.

3. Conclusion

Self-assembly of MWCNT with *Shewanella oneidensis* MR-1 was observed in the presence of cyt *c*. The resulting aggregates have been used to build a bacterial biocomposite that promoted extracellular electron transfer reactions. From a conceptual point of view, the association of MWCNT and cyt *c* with bacteria makes an artificial biofilm that mimics electroactive biofilm. The fabrication of this artificial biofilm, or biofilm-like layers, is rapid and was applied to another bacteria, i.e. *Pseudomonas fluorescens*. Connecting electroactive bacteria to an electrode surface thus becomes easy and rapid, which opens new opportunities for the application of a large diversity of bacterial strains from the emerging field of synthetic biology in bioelectrochemical systems.

One important and still opened question is the possibility to stabilize the electrochemical response of the biocomposite for long-term experiments, a point that we will examine in further work.

Supplementary material: variation of the size distribution in time with a suspension containing *Shewanella oneidensis* MR-1, MWCNT and cyt *c*; reference spectra of individuals components; corresponding RAMAN spectra of cartography; Scanning electron micrographs of the biocomposite layer made from *S. oneidensis*, MWCNT and cyt *c*; amperometric current responses with (1) *Shewanella oneidensis* MR-1, (2) *Shewanella oneidensis* MR-1 and cyt *c*, (3) *Escherichia coli*, MWCNT and cyt *c*, (4) *Pseudomonas fluorescens*, MWCNT and cyt *c*.

Acknowledgements. The authors gratefully acknowledge E. Mcrae for careful reading of the manuscript, M. J. Stébé for dynamic light scattering experiments, and both L. Salsi and J. Poali for SEM imaging. S. P. acknowledges the French Ministry of Higher Education (MRES) for the PhD grant.

References

- [1] M.C. Potter, Electrical effects accompanying the decomposition of organic compounds, *Proc. R. Soc. London. Ser. B. Contain. Pap. a Biol. Character.* 84 (1911) 260–276.
- [2] D.R. Bond, D.E. Holmes, L.M. Tender, D.R. Lovley, Electrode-Reducing Microorganisms That Harvest Energy from Marine Sediments, *Science* (80-.). 295 (2002) 483–485. doi:10.1126/science.1066771.
- [3] U. Schröder, Discover the possibilities: microbial bioelectrochemical systems and the revival of a 100-year-old discovery, *J. Solid State Electrochem.* 15 (2011) 1481–1486. doi:10.1007/s10008-011-1395-7.
- [4] Y.A. Gorby, S. Yanina, J.S. McLean, K.M. Rosso, D. Moyles, A. Dohnalkova, et al., Electrically conductive bacterial nanowires produced by *Shewanella oneidensis* strain MR-1 and other microorganisms., *Proc. Natl. Acad. Sci. U. S. A.* 103 (2006) 11358–63. doi:10.1073/pnas.0604517103.
- [5] G. Reguera, K.D. McCarthy, T. Mehta, J.S. Nicoll, M.T. Tuominen, D.R. Lovley, Extracellular electron transfer via microbial nanowires., *Nature.* 435 (2005) 1098–1101. doi:10.1038/nature03661.
- [6] H.J. Kim, H.S. Park, M.S. Hyun, I.S. Chang, M. Kim, B.H. Kim, A mediator-less microbial fuel cell using a metal reducing bacterium, *Shewanella putrefaciens*, *Enzyme Microb. Technol.* 30 (2002) 145–152. doi:10.1016/S0141-0229(01)00478-1.
- [7] N.S. Malvankar, S.E. Yalcin, M.T. Tuominen, D.R. Lovley, Visualization of charge propagation along individual pili proteins using ambient electrostatic force microscopy, *Nat. Nanotechnol.* 9 (2014) 1012–1017. doi:10.1038/nnano.2014.236.
- [8] S. Pirbadian, S.E. Barchinger, K.M. Leung, H.S. Byun, Y. Jangir, R. a. Bouhenni, et al., *Shewanella oneidensis* MR-1 nanowires are outer membrane and periplasmic extensions of the extracellular electron transport components, *Proc. Natl. Acad. Sci.* 111 (2014) 1–6. doi:10.1073/pnas.1410551111.
- [9] R.J. Steidl, S. Lampa-Pastirk, G. Reguera, Mechanistic stratification in electroactive biofilms of *Geobacter sulfurreducens* mediated by pilus nanowires, *Nat. Commun.* 7 (2016) 12217. doi:10.1038/ncomms12217.
- [10] M.D. Yates, S.M. Strycharz-Glaven, J.P. Golden, J. Roy, S. Tsoi, J.S. Erickson, et al., Measuring conductivity of living *Geobacter sulfurreducens* biofilms, *Nat. Nanotechnol.* 11 (2016) 910–913. doi:10.1038/nnano.2016.186.
- [11] S. Lampa-Pastirk, J.P. Veazey, K.A. Walsh, G.T. Feliciano, R.J. Steidl, S.H. Tessmer, et al., Thermally activated charge transport in microbial protein nanowires., *Sci. Rep.* 6 (2016) 23517. doi:10.1038/srep23517.
- [12] M.Y. El-Naggar, G. Wanger, K.M. Leung, T.D. Yuzvinsky, G. Southam, J. Yang, et al., Electrical transport along bacterial nanowires from *Shewanella oneidensis* MR-1., *Proc. Natl. Acad. Sci. U. S. A.* 107 (2010) 18127–18131. doi:10.1073/pnas.1004880107.
- [13] M.D. Yates, J. Golden, J. Roy, S.M. Strycharz-Glaven, S. Tsoi, J. Erickson, et al., Thermally Activated Long Range Electron Transport in Living Biofilms, *Phys. Chem. Chem. Phys.* 17 (2015) 32564–32570. doi:10.1039/C5CP05152E.

- [14] H. Wang, J. Park, Z.J. Ren, Practical Energy Harvesting for Microbial Fuel Cells: A Review, *Environ. Sci. Technol.* (2015) 150211042126005. doi:10.1021/es5047765.
- [15] B.E. Logan, K. Rabaey, Conversion of wastes into bioelectricity and chemicals by using microbial electrochemical technologies., *Science*. 337 (2012) 686–90. doi:10.1126/science.1217412.
- [16] D.R. Lovley, K.P. Nevin, Electrobiocommodities : powering microbial production of fuels and commodity chemicals from carbon dioxide with electricity, *Curr. Opin. Biotechnol.* 24 (2013) 385–390. doi:10.1016/j.copbio.2013.02.012.
- [17] X.C. Abrevaya, N.J. Sacco, M.C. Bonetto, A. Hilding-Ohlsson, E. Cortón, Analytical applications of microbial fuel cells. Part II: Toxicity, microbial activity and quantification, single analyte detection and other uses., *Biosens. Bioelectron.* 63C (2015) 591–601. doi:10.1016/j.bios.2014.04.053.
- [18] C. Pfeffer, S. Larsen, J. Song, M. Dong, F. Besenbacher, R.L. Meyer, et al., Filamentous bacteria transport electrons over centimetre distances, *Nature*. (2012) 10–13. doi:10.1038/nature11586.
- [19] N.S. Malvankar, D.R. Lovley, Microbial nanowires for bioenergy applications, *Curr. Opin. Biotechnol.* 27 (2014) 88–95. doi:10.1016/j.copbio.2013.12.003.
- [20] M. a. Rosenbaum, A.W. Henrich, Engineering microbial electrocatalysis for chemical and fuel production, *Curr. Opin. Biotechnol.* 29 (2014) 93–98. doi:10.1016/j.copbio.2014.03.003.
- [21] T. Krieg, A. Sydow, U. Schröder, J. Schrader, D. Holtmann, Reactor concepts for bioelectrochemical syntheses and energy conversion, *Trends Biotechnol.* 32 (2014) 645–655. doi:10.1016/j.tibtech.2014.10.004.
- [22] S. Wu, P. Liang, C. Zhang, H. Li, K. Zuo, X. Huang, Enhanced performance of microbial fuel cell at low substrate concentrations by adsorptive anode, *Electrochim. Acta.* 161 (2015) 245–251. doi:10.1016/j.electacta.2015.02.028.
- [23] L. Peng, S.-J. You, J.-Y. Wang, Carbon nanotubes as electrode modifier promoting direct electron transfer from *Shewanella oneidensis*., *Biosens. Bioelectron.* 25 (2010) 1248–51. doi:10.1016/j.bios.2009.10.002.
- [24] M. Picot, L. Lapinsonnière, M. Rothballer, F. Barrière, Graphite anode surface modification with controlled reduction of specific aryl diazonium salts for improved microbial fuel cells power output., *Biosens. Bioelectron.* 28 (2011) 181–8. doi:10.1016/j.bios.2011.07.017.
- [25] S. a Patil, K. Hasan, D. Leech, C. Hägerhäll, L. Gorton, Improved microbial electrocatalysis with osmium polymer modified electrodes., *Chem. Commun. (Camb)*. 48 (2012) 10183–5. doi:10.1039/c2cc34903e.
- [26] H.R. Luckarift, S.R. Sizemore, J. Roy, C. Lau, G. Gupta, P. Atanassov, et al., Standardized microbial fuel cell anodes of silica-immobilized *Shewanella oneidensis*., *Chem. Commun.* 46 (2010) 6048–6050. doi:10.1039/c0cc01255f.
- [27] W. Ghach, M. Etienne, V. Urbanova, F.P.A. Jorand, A. Walcarius, Sol–gel based “artificial” biofilm from *Pseudomonas fluorescens* using bovine heart cytochrome c as electron mediator, *Electrochem. Commun.* 38 (2014) 71–74.

doi:10.1016/j.elecom.2013.11.001.

- [28] Y.-C. Yong, Y.-Y. Yu, X. Zhang, H. Song, Highly active bidirectional electron transfer by a self-assembled electroactive reduced-graphene-oxide-hybridized biofilm., *Angew. Chem. Int. Ed. Engl.* 53 (2014) 4480–3. doi:10.1002/anie.201400463.
- [29] X. Jiang, J. Hu, A.M. Lieber, C.S. Jackan, J.C. Biffinger, L.A. Fitzgerald, et al., Nanoparticle facilitated extracellular electron transfer in microbial fuel cells., *Nano Lett.* 14 (2014) 6737–42. doi:10.1021/nl503668q.
- [30] A.Y. Chen, C. Zhong, T.K. Lu, Engineering Living Functional Materials, *ACS Synth. Biol.* 4 (2015) 8–11. doi:10.1021/sb500113b.
- [31] A.Y. Chen, Z. Deng, A.N. Billings, U.O.S. Seker, M.Y. Lu, R.J. Citorik, et al., Synthesis and patterning of tunable multiscale materials with engineered cells., *Nat. Mater.* 13 (2014) 515–23. doi:10.1038/nmat3912.
- [32] I. Willner, M. Lion-Dagan, S. Marx-Tibbon, E. Katz, Bioelectrocatalyzed Amperometric Transduction of Recorded Optical Signals Using Monolayer-Modified Au-Electrodes1, *J. Am. Chem. Soc.* 117 (1995) 6581–6592. doi:10.1021/ja00129a023.
- [33] R. Dronov, D.G. Kurth, H. Möhwald, R. Spricigo, S. Leimkühler, U. Wollenberger, et al., Layer-by-layer arrangement by protein-protein interaction of sulfite oxidase and cytochrome c catalyzing oxidation of sulfite, *J. Am. Chem. Soc.* 130 (2008) 1122–1123. doi:10.1021/ja0768690.
- [34] A. Scotti, W. Liu, J.S. Hyatt, E.S. Herman, H.S. Choi, J.W. Kim, et al., The CONTIN algorithm and its application to determine the size distribution of microgel suspensions, *J. Chem. Phys.* 142 (2015) 234905. doi:10.1063/1.4921686.
- [35] S. Kang, M. Herzberg, D.F. Rodrigues, M. Elimelech, Antibacterial effects of carbon nanotubes: size does matter!, *Langmuir.* 24 (2008) 6409–13. doi:10.1021/la800951v.
- [36] V.K.K. Upadhyayula, S. Deng, M.C. Mitchell, G.B. Smith, Application of carbon nanotube technology for removal of contaminants in drinking water: A review, *Sci. Total Environ.* 408 (2009) 1–13. doi:10.1016/j.scitotenv.2009.09.027.
- [37] M. Okada, N.I. Smith, A.F. Palonpon, H. Endo, S. Kawata, M. Sodeoka, et al., Label-free Raman observation of cytochrome c dynamics during apoptosis., *Proc. Natl. Acad. Sci. U. S. A.* 109 (2012) 28–32. doi:10.1073/pnas.1107524108.
- [38] M. Patila, I. V. Pavlidis, E.K. Diamanti, P. Katapodis, D. Gournis, H. Stamatis, Enhancement of cytochrome c catalytic behaviour by affecting the heme environment using functionalized carbon-based nanomaterials, *Process Biochem.* 48 (2013) 1010–1017. doi:10.1016/j.procbio.2013.04.021.
- [39] E. Dague, J. Duval, F. Jorand, F. Thomas, F. Gaboriaud, Probing Surface Structures of *Shewanella* spp. by Microelectrophoresis, *Biophys. J.* 90 (2006) 2612–2621. doi:10.1529/biophysj.105.068205.
- [40] K.J.M. Bishop, C.E. Wilmer, S. Soh, B.A. Grzybowski, Nanoscale forces and their uses in self-assembly, *Small.* 5 (2009) 1600–1630. doi:10.1002/smll.200900358.
- [41] R.J. Narayan, C.J. Berry, R.L. Brigmon, Structural and biological properties of carbon nanotube composite films, *Mater. Sci. Eng. B.* 123 (2005) 123–129. doi:10.1016/j.mseb.2005.07.007.

- [42] S.K. Manna, S. Sarkar, J. Barr, K. Wise, E. V. Barrera, O. Jejelowo, et al., Single-Walled Carbon Nanotube Induces Oxidative Stress and Activates Nuclear Transcription Factor- κ B in Human Keratinocytes, *Nano Lett.* 5 (2005) 1676–1684. doi:10.1021/nl0507966.
- [43] A. a Shvedova, E.R. Kisin, R. Mercer, A.R. Murray, V.J. Johnson, A.I. Potapovich, et al., Unusual inflammatory and fibrogenic pulmonary responses to single-walled carbon nanotubes in mice., *Am. J. Physiol. Lung Cell. Mol. Physiol.* 289 (2005) L698-708. doi:10.1152/ajplung.00084.2005.
- [44] S. Xu, Y. Jangir, M.Y. El-Naggar, Disentangling the roles of free and cytochrome-bound flavins in extracellular electron transport from *Shewanella oneidensis* MR-1, *Electrochim. Acta.* 198 (2016) 49–55. doi:10.1016/j.electacta.2016.03.074.

Figure captions

Scheme 1. Protocol for self-assembly of bacteria with carbon nanotubes in the presence of cytochrome *c* before deposition on electrodes for bioelectrochemistry.

Figure 1. (A) Pictures and (B) Size distribution diagrams determined by dynamic light scattering of a 1 mM KCl solution after 2 h at room temperature with: (a) *Shewanella oneidensis* MR-1, (b) multi-walled carbon nanotubes (MWCNT), (c) *Shewanella oneidensis* MR-1 and MWCNT, (d) *Shewanella oneidensis* MR-1 and cytochrome *c*, (e) MWCNT and cytochrome *c*, (f) *Shewanella oneidensis* MR-1, MWCNT and cytochrome *c* and (g) *Shewanella oneidensis* MR-1, MWCNT and bovine serum albumin. Data are extracted from a global distribution in volume and the apparent diameter is the D_{50} value with its interquartile range (IQR).

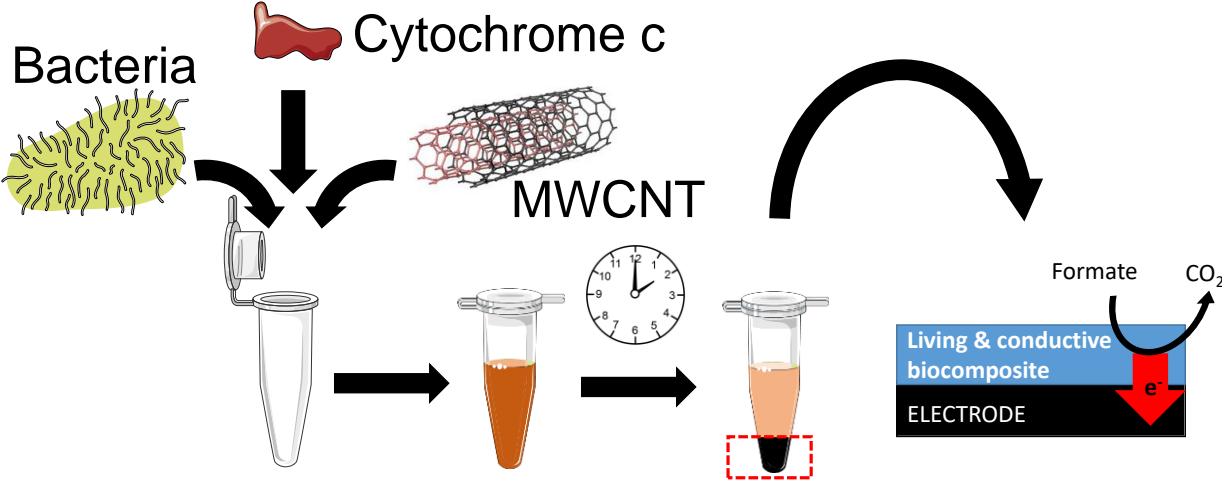
Figure 2. Scanning electron microscopy of the aggregates obtained after two hours at room temperature with (A) *Shewanella oneidensis* MR-1, (B) *Shewanella oneidensis* MR-1 and MWCNT and (C) *Shewanella oneidensis* MR-1, cytochrome *c* and MWCNT. Each system have been previously diluted and filtered. Samples were filtered on 0.22 μm membrane filters and fixed afterward with glutaraldehyde 2.5% in sodium cacodylate buffer (pH 7.2). A washing step in sodium cacodylate buffer for 20 min was performed before a dehydrating step in an alcohol gradient for 70 min. After preparation, samples were dried then metallized for the characterization with a Cambridge Stereoscan S240 SEM at an acceleration voltage of 1 kV.

Figure 3. (A&D) Optical images and Raman cartography integrating (B&E) G' band of carbon nanotubes at 2700 cm^{-1} and (C&F) cytochrome *c* band at 755 cm^{-1} on composite materials made of (A – C) MWCNT and cytochrome *c* or (D – F) *Shewanella oneidensis*, MWCNT and cytochrome *c*.

Figure 4. Scanning electron microscopy of the biocomposite layer made from (A&B) *Shewanella oneidensis* and MWCNT and (C&D) *Shewanella oneidensis*, MWCNT and cytochrome *c*. Samples were dropped on a glassy carbon plate without any further preparation and observed with a Hitachi S-4800 SEM at an acceleration voltage of 1 kV.

Figure 5. (A) Cyclic voltammograms measured with the biocomposites made of *Shewanella oneidensis* MR-1 and MWCNT, in the absence (curve a) and in the presence (curve b) of cytochrome *c*, in the absence (curve a,b) and in the presence (curve c) of 0.3 mM formate (B) Amperometric current responses to several additions (arrows) of 0.1 mM of formate measured with a glassy carbon electrode modified with *Shewanella oneidensis* MR-1 and MWCNT (curve a) or with *S. oneidensis* MR-1, MWCNT and cytochrome *c* (curve b). (C) Amperometric current response to 50 mM formate measured with a graphite felt electrode impregnated with a biocomposite made from *Shewanella oneidensis* MR-1, MWCNT and cytochrome *c* (curve a) or only *Shewanella oneidensis* MR-1 (curve b). The measurements were performed in 50 mM phosphate buffer (pH 7) at room temperature. Cyclic voltammograms were obtained at 50 mV s⁻¹. All amperometric curves were recorded at + 0.35 V versus an Ag/AgCl reference electrode. Note that experiments reported in curves b and c of Figure 5A have been performed respectively before and after the chronoamperometric measurement shown in curve b of Figure 5B.

Scheme



Scheme 1

Figures

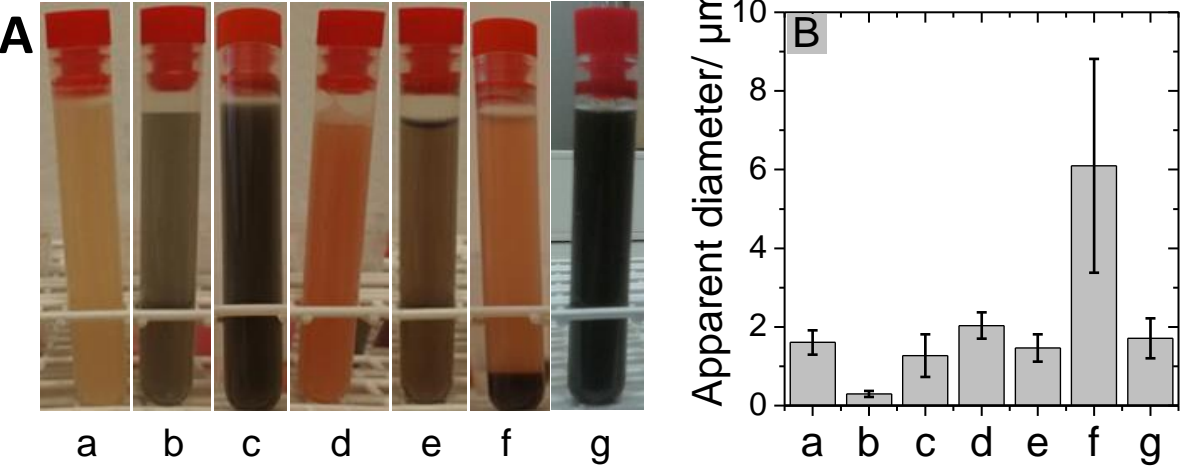


Figure 1

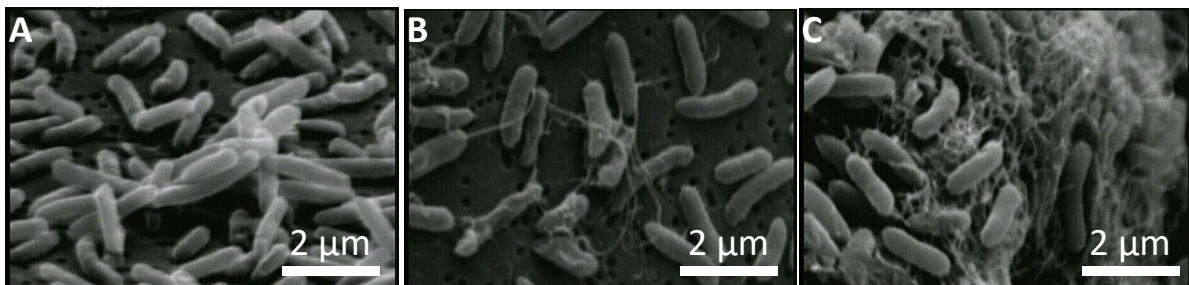


Figure 2

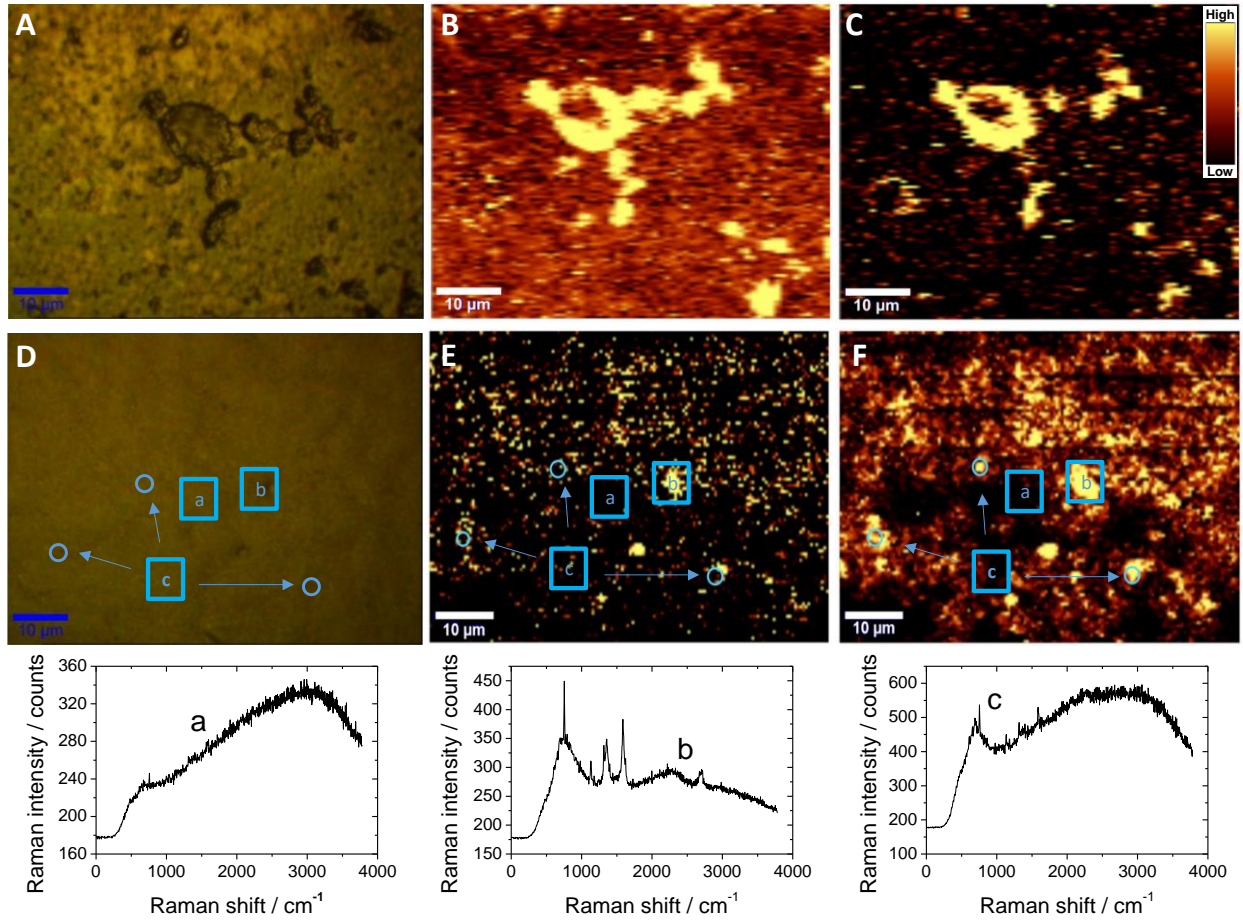


Figure 3

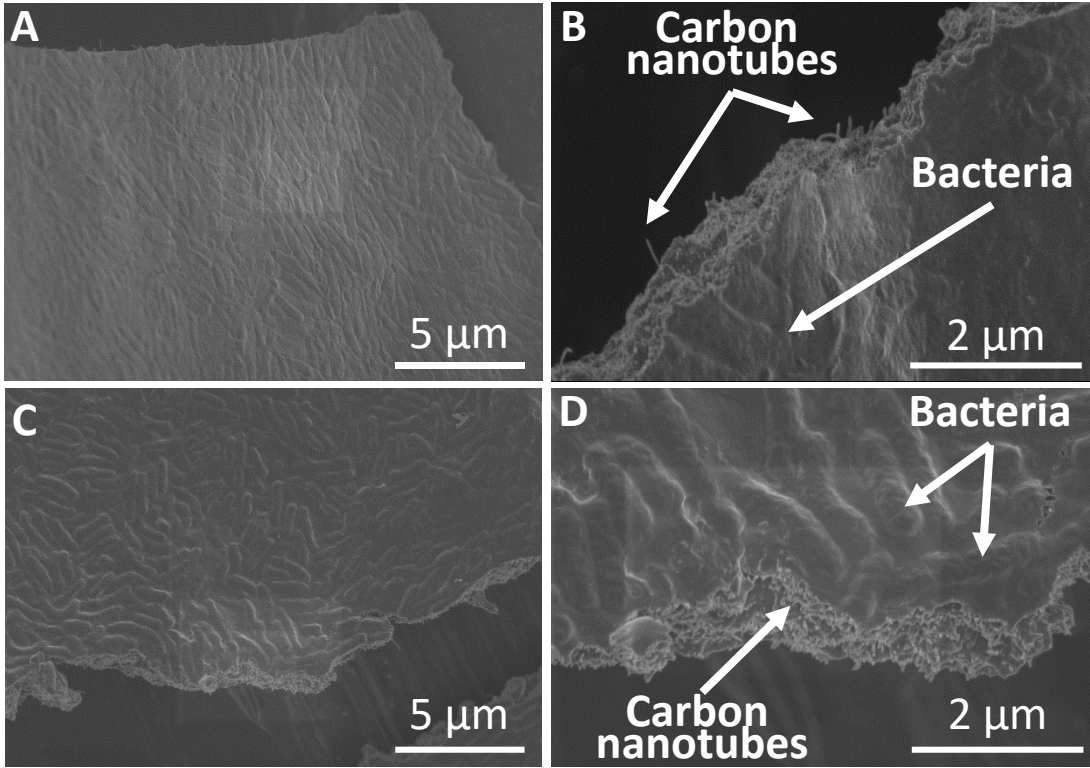


Figure 4

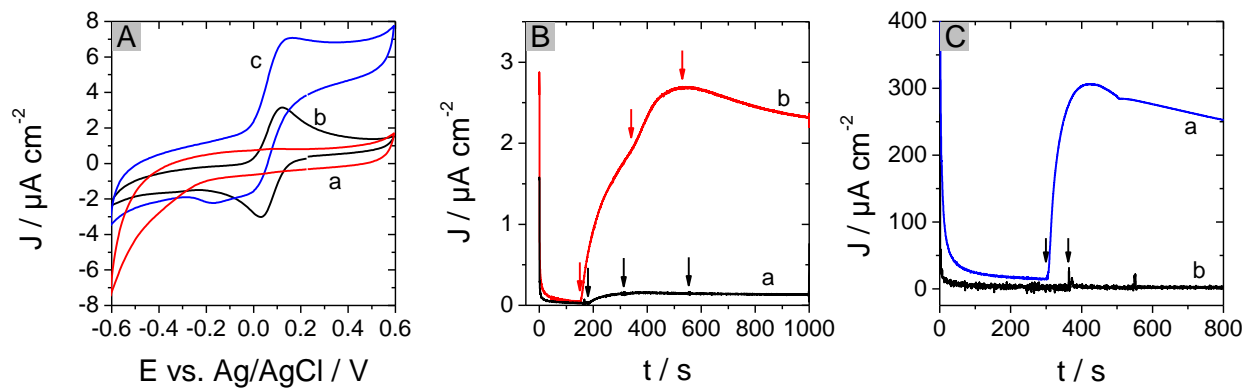


Figure 5

Table 1. Absorbance measured at 550 nm, final concentration of cytochrome *c* (cyt *c*) and amount of immobilized cyt *c* after 2 h self-assembly between *Shewanella oneidensis* MR-1 (1×10^9 cell mL⁻¹), MWCNT (1 mg mL⁻¹) and cyt *c* (initial concentration between 0.05 and 0.8 mM) in 1 mM KCl or 0.4 M phosphate buffer. Standard deviation is estimated from triplicate measurements.

	1 mM KCl						0.4 M phosphate buffer
Initial cyt <i>c</i> concentration (mM)	0.05	0.1	0.2	0.2	0.4	0.8	0.200
Absorbance at 550 nm	3.54 ± 0.08	3.91 ± 0.06	0.60 ± 0.03	0.61 ± 0.03	1.37 ± 0.03	2.91 ± 0.04	>4
Final cyt <i>c</i> concentration (mM)	nd	nd	0.153 ± 0.008	0.154 ± 0.008	0.350 ± 0.008	0.744 ± 0.01	n.d.
Amount of immobilized cyt <i>c</i> (10 ⁻⁹ mole)	nd	nd	23 ± 4	23 ± 4	25 ± 4	28 ± 5	n.d.